Construction and Calibration of a Low-Cost 3D Laser Scanner with 360° Field of View for Mobile Robots

Jorge L. Martínez, Jesús Morales, Antonio J. Reina, Anthony Mandow,
Alejandro Pequeño-Boter* and Alfonso García-Cerezo

Universidad de Málaga, Andalucía Tech, Dpto. Ingeniería de Sistemas y Automática, 29071-Málaga, Spain
Email: jlmartinez@uma.es, Tel: (+34) 951 952322.
*Ingeniería UNO, Calle Alcalde Garret y Souto, 38, 29006-Málaga, Spain.
Email: info@ingenieriauno.com; Tel: (+34) 952 038227.

***Abstract*—Navigation of many mobile robots relies on environmental information obtained from three-dimensional (3D) laser scanners. This paper presents a new 360° field-of-view 3D laser scanner for mobile robots that avoids the high cost of commercial devices. The 3D scanner is based on spinning a Hokuyo UTM-30LX-EX two-dimensional (2D) rangefinder around its optical center. The proposed design profits from lessons learned with the development of a previous 3D scanner with pitching motion. Intrinsic calibration of the new device has been performed to obtain both temporal and geometric parameters. The paper also shows the integration of the 3D device in the outdoor mobile robot Andabata.**

I. Introduction

Nowadays, navigation of many mobile robots relies on environmental information obtained from 3D laser scanners. Examples include planetary investigation [1], natural terrain exploration [2], and search & rescue [3]. However, due to the cost of commercial solutions, many robotics researchers build their own 3D scanners by adding a rotation to standard 2D rangefinders [4].

The most employed commercial 3D rangefinders with 360° field of view in mobile robotics are provided by Velodyne with multi-beam models HDL-64E [5] [6] [7] [8] and HDL-32E [9] [10] [11]. These models differ mainly in the number of laser/detectors located in the rotating head: 64 and 32, respectively. The main advantage of these sensors is the high acquisition rate that makes them suitable for vehicles moving at high speeds. However, they have a limited vertical resolution and are much more expensive than actuated 2D sensors [12].

This paper presents the design and development of UNOmotion, a lightweight and low-cost 3D laser scanner (see Fig. 1) based on spinning an off-the-shelf 2D rangefinder. The design of UNOmotion accomplishes the following specifications: the optical center of the scanner coincides with that of the 2D device, the mechanism does not interfere with the measurement planes, and continuous rolling motion for efficient 3D scanning time.

Fig. 1. The new 3D rangefinder UNOmotion for mobile robotics.

With respect to our previous design [13], where a Hokuyo UTM-30LX unit was pitched around its optical center, the following aspects have been improved:

- the design targets the new Hokuyo UTM-30LX-EX, which includes additional features such as intensity data,
- the mechanical system has been simplified and no wires are now visible,
- the 2D sensor and the motion controller for the extra rotation can be accessed independently for a more flexible use, and
- the field of view has been widened to 360° while scan-time has been reduced.

The paper is organized as follows. Next section describes the new 3D laser rangefinder and compares its specifications with Velodyne's models. Section III offers intrinsic calibration results for the developed device. The application of the sensor to mobile robotics is presented in section IV. The paper ends with conclusions, acknowledgments and references.

II. Sensor construction

The 3D laser rangefinder is based on spinning the new Hokuyo UTM–30LX–EX laser scanner and, consequently, inherits its measurement characteristics. This 2D sensor has compact dimensions ($62 \times 62 \times 87$ mm) and only weights 400 g. A 2D scan with a field of view of $270°$ and an angular resolution of $0.25°$ can be obtained in 25 ms. It has a maximum scanning range of 30 m and a minimum range of 0.1 m. It is powered through a 12 V DC power supply with a nominal current of 0.7 A with peaks of 1 A. With respect to the previous model UTM–30LX, the new 2D sensor has IP67 protection, multi-echo functionality, Ethernet interface and also provides intensity information.

UNOmotion weights 1.9 kg and its maximum dimensions are $125 \times 170 \times 222$ mm. The main parts of UNOmotion are the rotating head, which houses the 2D rangefinder, and the base, which provides the extra rotation (see Fig. 2).

By aligning the extra vertical rotation axis with the optical center of the 2D device, the 3D scanner maintains the same minimum range as the 2D unit and avoids offsets in computing Cartesian coordinates [14]. Scan acquisition rate is twice the rotation rate because a scan is completed every $180°$. Furthermore, the roll angle resolution can be increased or decreased depending on rotation speed.

The blind zone of 2D sensor, which is $90°$ wide, is situated downward to avoid interferences with the base. In this way, the blind zone of the 3D scanner forms a cone (see Fig. 3). The radius of the cone base is equal to the height h of the optical center.

The main components of the base are depicted in Fig. 2. The DC servomotor is equipped with a gear unit of 3.75:1 and an optical incremental encoder of 4000 pulses per revolution. Accurate motion transmission to the head is implemented by a ball bearing with pulleys connected by a timing belt. In particular, the motor and bearing pulleys have 20 and 60 teeth, respectively. Therefore, a complete turn of the 2D sensor comprises 45000 encoder pulses. Moreover, unrestrained rotation is implemented with a slip ring that allows power and data transmission.

This motor is actuated through a full H-bridge power stage with pulse width modulation (PWM). The motion controller consists of a 16-bit digital signal processor (DSP) with a PWM generator, quadrature decoders, universal asynchronous receiver-transmitter (UART) interface with a universal serial bus (USB) converter cable, and digital input/output ports. A binary optical sensor serves to signal the zero rotation angle for the incremental encoder. The goals of the controller are to guarantee a constant spinning velocity and to synchronize the extra rotation with 2D data acquisition.

A functional diagram of UNOmotion is shown in Fig. 4. The 2D sensor and the motion controller can be accessed independently by the host computer through different communication ports. The Ethernet link of the Hokuyo is used for continuously sending scans and also for sensor configuration. The synchronization signal of the 2D sensor is captured by the motion controller, that sends the encoder position along with its internal time to the the host computer via USB. The computer, in turn, specifies the spinning speed to the motion controller through USB.

Table I shows relevant specifications of Velodyne's models in comparison with UNOmotion. It can be observed that both vertical resolution and vertical field of view are favorable to UNOmotion. Nevertheless, the maximum range and the scan acquisition rate are smaller.

III. Intrinsic calibration

Intrinsic parameters are those related with the acquisition mechanism of the 3D sensor. To obtain accurate Cartesian

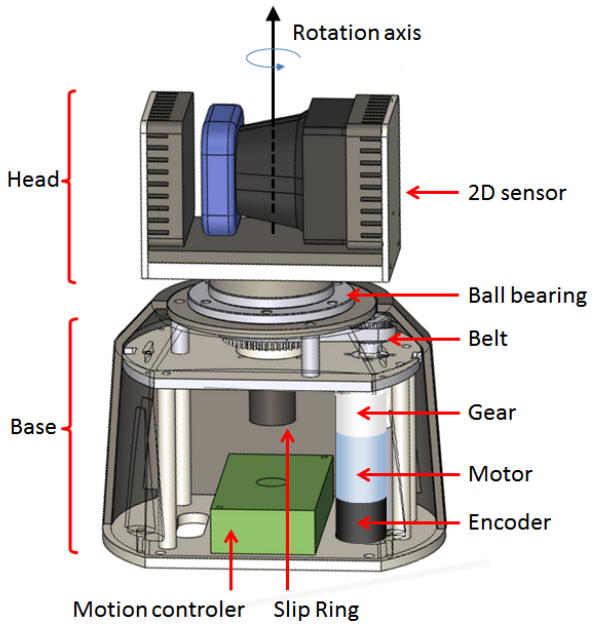

Fig. 2. Main components of the 3D laser scanner. Cabling and other details are not shown.

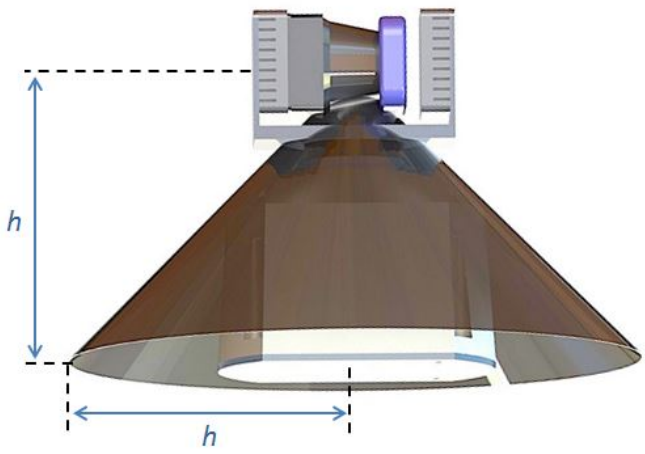

Fig. 3. Blind cone produced by the rotation of the blind area of the 2D scanner.

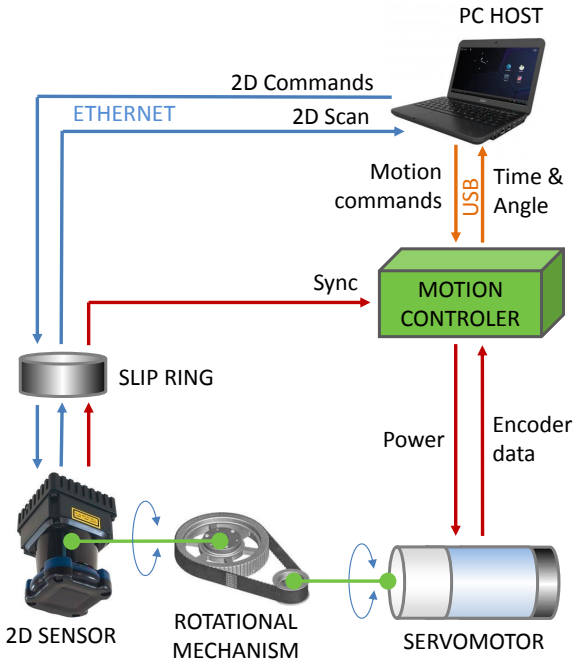

Fig. 4. Functional diagram of the 3D laser rangefinder.

Specifications	HDL-64E	HDL-32E	UNOmotion
Vertical resolution	0.42°	1.33°	0.25°
Vertical field of view	26.8°	41.34°	67.5°
Maximum range	120 m	70 m	30 m
Scan acquisition rate	5 – 20 Hz	10 Hz	0 – 1.48 Hz
Horizontal resolution	0.09 – 0.35°	0.16°	0 – 6.67°

TABLE I
COMPARISON OF UNOMOTION WITH VELODYNE'S MODELS.

coordinates requires calibration of both temporal (i.e., synchronization) and geometric parameters [15]. Experimental calibration data consists of a set of consecutive scans of a small room with stairs (see Fig. 5). These have been acquired at a rolling speed of 0.465 rad/s, but recorded data also includes 2D scans with zero rotation speed before and after motion. Data synchronization is performed in the first place. Then, geometric parameters can be obtained.

A. Computing Cartesian coordinates

Let the optical center O_2 of the 2D device be placed in its rotating mirror. Let the Z_2 axis of the frame associated to the 2D device be coincident with the mirror rotation axis, and the Y_2 axis be aligned with the centerline of the measurement plane. A point of the 2D device is given by its polar coordinates: angle α, which is assumed to be null in the X_2 direction, and range ρ.

The reference frame $OXYZ$ of the 3D sensor is defined as coincident with that of the 2D device when the extra rotation angle around Y_2 is $\theta = 0°$. Then, the Cartesian coordinates of the point cloud can be computed from ρ, α and θ as:

$$\begin{pmatrix} x \\ y \\ z \end{pmatrix} = \rho \begin{pmatrix} C(\alpha)\,C(\theta) \\ S(\alpha) \\ C(\alpha)\,S(\theta) \end{pmatrix} \quad (1)$$

where $C(\cdot)$ and $S(\cdot)$ stand for cosine and sine functions, respectively.

B. Data synchronization

Synchronization between rolling motion and 2D data acquisition requires that each 2D scan is stamped with an initial θ angle. Since 2D scans and θ angles are received by the host computer through different communication ports (see Fig. 4), it is necessary to synchronize messages from both sources.

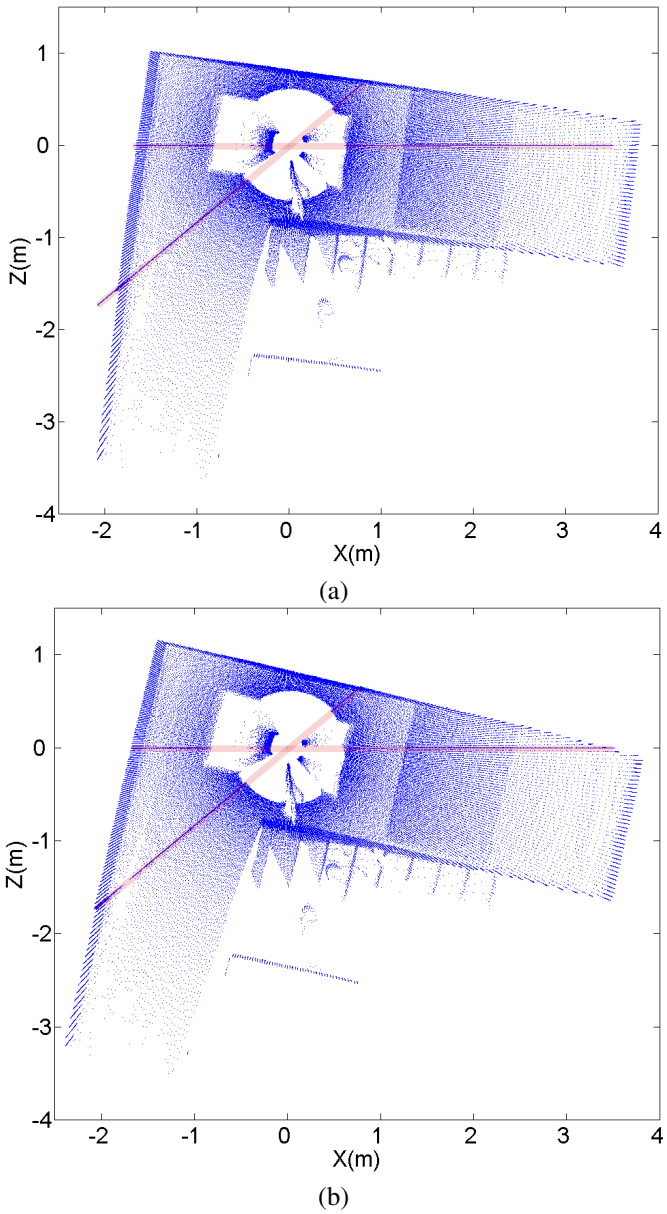

Fig. 5. X-Z projection of successive scans of a room, before (a) and after (b) data synchronization. Red lines outline 2D scans obtained before and after head motion.

The 2D sensor, which gives ranges from $\alpha = 225°$ to $\alpha = -45°$, signals a 1 ms low pulse each time its mirror passes through $\alpha = -90°$ (i.e., the middle of its blind zone). The motion controller captures the encoder position at the falling edge of this signal, and sends the corresponding θ to the computer along with its internal time.

2D scans obtained before and after head motion can be employed to perform data synchronization in a simple way. Synchronization errors provoke that Cartesian points computed with (1) for static scans do not match with those obtained with the head in motion. This can be appreciated in Fig. 5(a), where stopped points around $(x, z) = (3.5, 0)$ do not reach the actual wall on the right whereas those around $(-2, -1.7)$ fall beyond wall limits. Then, synchronization can be achieved by adjusting a delay between the Ethernet and USB messages so that static scans match, as illustrated in Fig. Fig. 5(b).

By applying this technique, the gap between USB and Ethernet messages has been calculated as 0.2 s, that corresponds to 8 times the 2D scanning time of 0.25 ms. This means that USB messages with θ angles are received sooner than their respective Ethernet messages with 2D scans. This relevant delay is explained because the portable computer employed in the experiment required an Ethernet-to-USB cable.

C. Geometric calibration

Small errors in the attachment of the 2D device to the rotating mechanism provokes that Y_2 is not perfectly aligned with Y (see Fig. 6). This misalignment provokes a distortion in the point cloud computed with (1).

Many intrinsic calibration methods for spinning actuated 2D scanners do not require specialized calibrated targets, e.g., [16]. For 3D scanners with a low-cost 2D laser rangefinder rotating on its optical center, the calibration method proposed in [14] can be employed to obtain mechanical misalignments in UNOmotion. Inherited measurement limitations from the 2D device prevent estimation of very small translation misalignments, so the calibration problem is reduced to obtaining boresight (i.e., orientation) parameters. Optimal angles β_0 and α_0, as defined in Fig. 6, are calculated by iterative maximization of both the flatness and the area of detected planar patches from a single 3D scan taken from an arbitrary position.

The following boresight calibration parameters: $\beta_0 = 0.5°$ and $\alpha_0 = -0.02°$ have been obtained with a single scan from the calibration experiment. After calibration, (2) –see equation below– can be employed to obtain 3D cartesian coordinates of a point in the 3D frame instead of (1), where $\Theta = \theta_0 + \theta$, and θ_0 represents the zero angle of the rotation mechanism. θ_0 is an extrinsic parameter that depends on the installation of the sensor on the mobile robot.

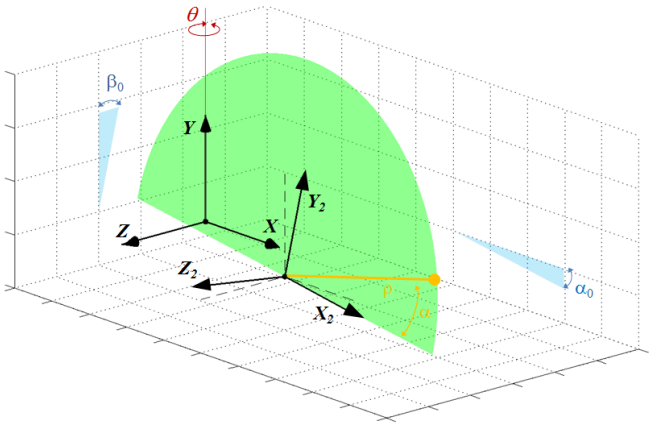

Fig. 6. Calibration angles.

Fig. 7. Illustration of UAV sensor mounting.

IV. Application to Mobile Robotics

The placement of the 3D laser scanner in a mobile robot is a relevant issue that should be studied. The preferred mounting configuration is vertical to minimize ball bearing and belt stress.

For terrestrial mobile robots, the sensor can be mounted at the top of the robot to take advantage of its 360° field of view. Increasing the height of the sensor improves the point of view, but the radius of the blind circle around the vehicle also grows proportionally (i.e., the cone base in Fig. 3).

For Unmanned Aerial Vehicles (UAVs), the 3D sensor can be placed upside-down at the bottom of the vehicle (see Fig. 7). In this way, the maximum scanning resolution can be pointing to the ground.

A. Installation in the mobile robot Andabata

The 3D device has been incorporated to the outdoor mobile robot Andabata (see Fig. 8). This battery-operated robot has a weight of 41 kg and its dimensions are 64 cm length, 50 cm width and 35 cm height.

$$\begin{pmatrix} x \\ y \\ z \end{pmatrix} = \begin{pmatrix} C(\alpha_0)\,C(\Theta) + S(\beta_0)\,S(\alpha_0)\,S(\Theta) & C(\alpha_0)\,S(\beta_0)\,S(\Theta) - C(\Theta)\,S(\alpha_0) \\ C(\beta_0)\,S(\alpha_0) & C(\beta_0)\,C(\alpha_0) \\ C(\alpha_0)\,S(\Theta) - S(\beta_0)\,C(\Theta)\,S(\alpha_0) & -S(\alpha_0)\,S(\Theta) - C(\alpha_0)\,S(\beta_0)\,C(\Theta) \end{pmatrix} \begin{pmatrix} \rho\,C(\alpha) \\ \rho\,S(\alpha) \end{pmatrix} \quad (2)$$

Fig. 8. The 3D laser scanner mounted on the outdoor mobile robot Andabata.

The onboard computer with an Intel Core i7 4771 processor (3.5 GHz, 8 MB cache, 16 GB RAM) employs the Robot Operating System (ROS) [17]. Data synchronization, as described in section III-B, provides a null gap between USB and Ethernet messages for this computer.

UNOmotion has been installed centered on a 20 cm height mounting to avoid shadows from the robot. This mounting also serves to attach a mobile phone that provides bearing, GPS data, roll and pitch angles to Andabata.

Two extrinsic calibration parameters for this sensor position have been obtained by aligning the mobile robot to a wall of a corridor and extracting planes from the acquired 3D point cloud using the RANSAC method [18]. The main detected planes are those associated to the walls, the floor an the ceiling (see Fig. 9).

The first parameter is the height of the origin of the 3D laser frame above the ground. The value of 72.3 cm has been obtained using the distance to the floor plane, which also corresponds to the radius of the blind circle around the robot. The second parameter is the angle θ_0 employed to align the longitudinal axis of the vehicle with the X axis of the 3D device. It has been estimated as $-150.5°$ using the normal vectors of the wall planes.

The point clouds obtained with (2) from two 3D scans taken inside and outside of a warehouse with the robot stopped are shown in Fig. 10. Points are colored according to their ranges, with points closer to the mobile robot shown in red and farther in blue. For both 3D scans, roll resolution has been set to $0.67°$, with an acquisition time of 6.75 s.

The silhouette of a car and persons can be recognized in

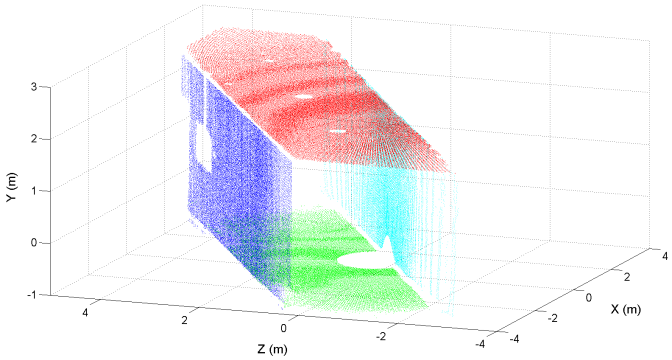

Fig. 9. The main planes extracted from the 3D point cloud of a corridor.

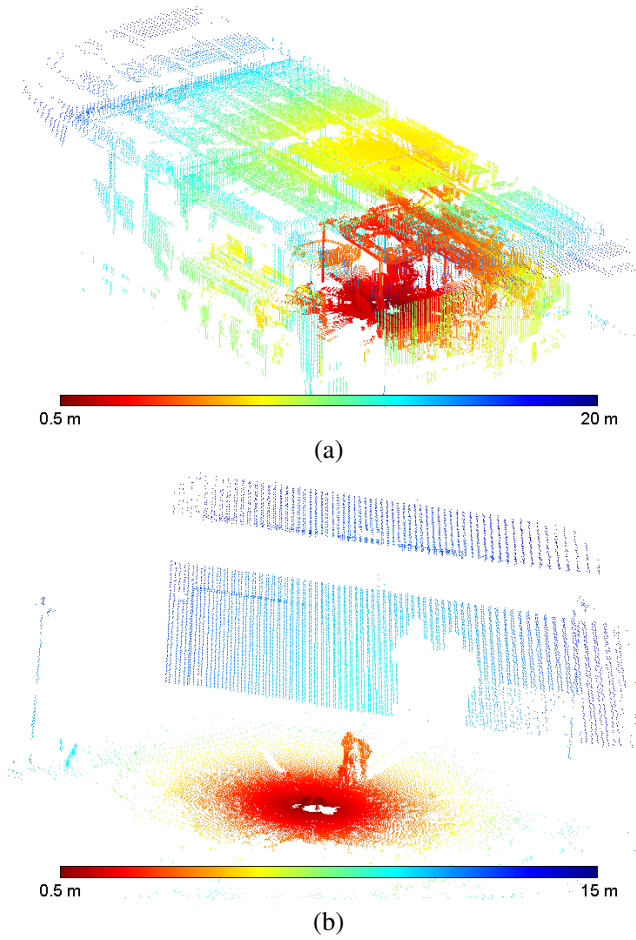

Fig. 10. Point clouds inside (a) and outside (b) of a warehouse.

Fig 10 (a) and (b), respectively. Under direct sunlight, almost all the ranges for the outdoor scenario are under 15 m as it can be observed in Fig 10 (b).

V. Conclusions

This paper has described a new 3D laser scanner with 360° field of view for mobile robots that avoids the high cost from commercial solutions. The 3D sensor is based on rolling an off-the-shelf 2D rangefinder around its optical center. In

particular, the design targets the new Hokuyo UTM-30LX-EX. Calibration has been performed to obtain both temporal and geometric parameters of the new sensor.

With respect to our previous design with the pitching configuration, we have enhanced numerous aspects, including smaller scan-times and simpler mechanics. However, the decision of changing the 2D device for the newest model has not been as good as expected because of the reduced maximum range with direct sunlight.

Future work includes the employment of the point clouds to build local navigation maps [19] [20] for the mobile robot Andabata. It is also interesting to correct distortions in 3D scans when the vehicle moves on uneven terrain [12].

ACKNOWLEDGMENTS

This work was partially supported by the Spanish CICYT project DPI 2011-22443 and the Andalusian project PE-2010 TEP-6101.

REFERENCES

[1] C. H. Tong, T. D. Barfoot, and E. Dupuis, "Three-dimensional SLAM for mapping planetary work site environments," *Journal of Field Robotics*, vol. 29, no. 3, pp. 381–412, 2012.

[2] J. Serón, J. L. Martínez, A. Mandow, A. J. Reina, J. Morales, and A. García-Cerezo, "Automation of the arm-aided climbing maneuver for tracked mobile manipulators," *IEEE Transactions on Industrial Electronics*, vol. 61, no. 7, pp. 3638–3647, 2014.

[3] J. Pellenz, D. Lang, F. Neuhaus, and D. Paulus, "Real-time 3D mapping of rough terrain: A field report from disaster city," in *IEEE International Workshop on Safety Security and Rescue Robotics*, 2010, pp. 1–6.

[4] O. Wulf and B. Wagner, "Fast 3D scanning methods for laser measurement systems," in *Proc. International Conference on Control Systems and Computer Science*, Bucharest (Romania), 2003, pp. 312–317.

[5] N. Vaskevicius, A. Birk, K. Pathak, and S. Schwertfeger, "Efficient representation in three-dimensional environment modeling for planetary robotic exploration," *Advanced Robotics*, vol. 24, no. 8-9, pp. 1169–1197, 2010.

[6] A. Huang, M. Antone, E. Olson, L. Fletcher, D. Moore, S. Teller, and J. Leonard, "A high-rate, heterogeneous data set from the DARPA urban challenge," *International Journal of Robotics Research*, vol. 29, no. 13, pp. 1595–1601, 2010.

[7] N. Muhammad and S. Lacroix, "Loop closure detection using small-sized signatures from 3D LIDAR data," in *Proc. 9th IEEE International Symposium on Safety, Security, and Rescue Robotics*, Kyoto, Japan, 2011, pp. 333–338.

[8] N. Wojke and M. Häselich, "Moving vehicle detection and tracking in unstructured environments," in *Proc. IEEE International Conference on Robotics and Automation*, Saint Paul, USA, 2012, pp. 3082–3087.

[9] W. Grant, R. Voorhies, and L. Itti, "Finding planes in LiDAR point clouds for real-time registration," in *Proc. IEEE International Conference on Intelligent Robots and Systems*, Tokyo, Japan, 2013, pp. 4347–4354.

[10] T. Egawa, I. Samejima, Y. Nihei, S. Kagami, and H. Mizoguchi, "A tabletop objects observation method from mobile robot using kinect sensor," in *Proc. IEEE International Conference on Systems, Man, and Cybernetics*, Manchester, United Kingdom, 2013, pp. 2771–2776.

[11] J. Morales, J. L. Martínez, A. Mandow, A. Reina, J. Serón, and A. García-Cerezo, "Improving 3D scan matching time of the coarse binary cubes method with fast spatial subsampling," in *Proc. 39th Annual Conference of the IEEE Industrial Electronics Society*, Vienna, Austria, 2013, pp. 4168–4173.

[12] H. Almqvist, M. Magnusson, and A. Lilienthal, "Improving point cloud accuracy obtained from a moving platform for consistent pile attack pose estimation," *Journal of Intelligent and Robotic Systems: Theory and Applications*, vol. 75, no. 1, pp. 101–128, 2014.

[13] J. Morales, J. L. Martínez, A. Mandow, A. Pequeño-Boter, and A. García-Cerezo, "Design and development of a fast and precise low cost 3D laser rangefinder," in *Proc. IEEE International Conference on Mechatronics*, Istanbul, Turkey, 2011, pp. 621–626.

[14] J. Morales, J. L. Martínez, A. Mandow, A. J. Reina, A. Pequeño-Boter, and A. García-Cerezo, "Boresight calibration of construction misalignments for 3D scanners built with a 2D laser rangefinder rotating on its optical center," *Sensors*, vol. 14, no. 11, pp. 20 025–20 040, 2014.

[15] M. Sheehan, A. Harrison, and P. Newman, "Self-calibration for a 3D laser," *International Journal of Robotics Research*, vol. 31, no. 5, pp. 675–687, 2012.

[16] H. Alismail and B. Browning, "Automatic calibration of spinning actuated lidar internal parameters," *Journal of Field Robotics*, pp. 1–25, 2014.

[17] M. Quigley, B. Gerkey, K. Conley, J. Faust, T. Foote, J. Leibs, E. Berger, R. Wheeler, and A. Ng, "ROS: an open-source robot operating system," in *Workshop on Open Source Software, IEEE International Conference on Robotics and Automation*, Kobe, Japan, 2009, pp. 1–6.

[18] R. B. Rusu and S. Cousins, "3D is here: Point Cloud Library (PCL)," in *Proc. IEEE International Conference on Robotics and Automation*, Shanghai, China, 2011, pp. 1–4.

[19] J. L. Martínez, A. Mandow, A. Reina, T. J. Cantador, J. Morales, and A. García-Cerezo, "Navigability analysis of natural terrains with fuzzy elevation maps from ground-based 3D range scans," in *Proc. IEEE/RSJ International Conference on Intelligent Robots and Systems*, Tokyo, Japan, 2013, pp. 1576–1581.

[20] A. Reina, J. L. Martínez, A. Mandow, J. Morales, and A. García-Cerezo, "Collapsible cubes: Removing overhangs from 3D point clouds to build local navigable elevation maps," in *Proc. IEEE/ASME International Conference on Advanced Intelligent Mechatronics*, Besancon, France, 2014, pp. 1012–1017.